RESEARCH ARTICLE

Magnetohydrodynamic and Thermal Behaviour of Maxwell Fluids over Cylindrical Surfaces in Porous Media with Joule Heating Effects

K. Sudarmozhi[1,*]

[1] Department of Mathematics, Saveetha School of Engineering, Saveetha Institute of Medical and Technical Sciences (SIMATS), Chennai 602105, India

Abstract

This work examines steady, laminar, axisymmetric flow of an electrically conducting upper-convected Maxwell fluid over a stretching cylinder embedded in a Darcy porous medium, with Joule heating, viscous dissipation and Newtonian (conjugate) wall heating acting together. Similarity transformations reduce the momentum, energy and species equations to coupled nonlinear ordinary differential equations, which are solved with a fourth-order collocation method with residual control (bvp4c). In the limiting case of a flat sheet, the computed skin-friction coefficients agree with five published benchmark solutions to within 0.032%, and tolerance, mesh and domain-length tests confirm convergence. Raising the magnetic parameter from 0.5 to 1.0 increases the skin-friction coefficient by 13.37% and the Nusselt number by 10.61%, but lowers the Sherwood number by 6.73%. Raising the porous-medium parameter Po from 0.3 to 0.5 increases the skin friction by 6.10% and the Nusselt number by 2.41%, and a larger Maxwell (relaxation-time) parameter, from 0.1 to 0.3, gives 3.77% more skin friction and a 2.04% higher Nusselt number; both reduce the Sherwood number. Heat transfer is most sensitive to the wall-heating parameters: the Nusselt number rises by 16.86% when Ec increases from 0.3 to 0.5 and by a factor of about 5.3 when the Newtonian heating parameter increases from 0.1 to 0.3, whereas it varies non-monotonically with Pr. Increasing the Schmidt number from 2 to 4 raises the Sherwood number by 52.79%. The magnetic, porous and viscoelastic parameters thicken the thermal and concentration boundary layers, while a larger curvature parameter lowers the wall temperature but thickens the outer part of both layers. The results are relevant to polymer extrusion, wire and fibre coating, heat exchangers, chemical reactors and thermal management of electronic devices.

Keywords: joule heating, Maxwell fluid, Newtonian heating, stretching cylinder, porous medium, bvp4c.

Submitted: 06 September 2026
Revised: 08 October 2026
Accepted: 11 October 2026
Published: 20 October 2026

Vol. 2, **No.** 2, 2026.
10.62762/IJTSSE.2026.517065

***Corresponding author:**
K. Sudarmozhi
sudarmozhik1033.sse@saveetha.com

Citation
Sudarmozhi, K. (2026). Magnetohydrodynamic and Thermal Behaviour of Maxwell Fluids over Cylindrical Surfaces in Porous Media with Joule Heating Effects. *International Journal of Thermo-Fluid Systems and Sustainable Energy*, 2(2), 117–129.

© 2026 by the Author. Published by Institute of Central Computation and Knowledge. This is an open access article under the CC BY license (https://creativecommons.org/licenses/by/4.0/).

1 Introduction

Maxwell fluids are the simplest rate-type viscoelastic fluids. With a single relaxation time they reproduce the stress relaxation seen in polymer melts, polymer solutions and many biological and industrial liquids. Flows of such fluids over cylindrical surfaces arise in polymer extrusion, wire and fibre drawing, filtration through porous media and chemical reactors, where the coupled velocity, temperature and concentration fields govern process efficiency and product quality. In these processes an applied magnetic field can be used to control the flow, a porous matrix resists it, and the temperature distribution is set by Joule heating, viscous dissipation and the thermal condition at the wall. Most earlier studies of these effects dealt with flat or otherwise simpler geometries, or with other constitutive models. The cylindrical configuration considered here is closer to extrusion and fibre processing, but the governing equations then contain transverse-curvature terms that make the problem harder to treat.

Khan et al. [1] analysed irreversibility in Darcy-Forchheimer flow of a Newtonian fluid with Joule heating and showed that the magnetic field strongly affects both the flow and the entropy generation; fluid elasticity was not included. Sudarmozhi et al. [2] investigated Maxwell fluid flow over a porous stretching cylinder with heat generation and chemical reaction, and showed that the Maxwell and porosity parameters together retard the flow and thicken the thermal boundary layer; Joule heating and Newtonian heating were not considered.

Mahanthesh et al. [3] modelled heat transfer in a magneto-non-Newtonian material flowing in a circular tube with viscous and Joule heating and found that the heat transfer rate depends strongly on the magnetic and rheological parameters; their wall condition was a constant heat flux rather than Newtonian heating. Khedher et al. [4] studied the periodic behaviour of current density and heat-transfer amplitude for an electrically conducting fluid along a thermally magnetised cylinder with MHD and Joule heating, but the fluid was Newtonian and no porous medium was present. For Maxwell fluids, Ahmed et al. [5] examined thermally radiative swirling flow over a porous rotating disk with Joule heating, and Gangadhar et al. [6] considered the von Kármán viscous pump of a rotating disk in a magnetised Maxwell fluid. Both studies show how the magnetic field modifies Maxwell-fluid flow, but both are restricted to disk geometry and neither uses Newtonian heating.

Suraiah Palaiah et al. [7] analysed the magnetised dissipative Soret effect on a chemically reactive Maxwell fluid over a stretching sheet with Joule heating and showed that the Soret number and the reaction rate alter the flow. Zaidi and Mohyud-Din [8] treated Joule heating and MHD in the wall-jet flow of an upper-convected Maxwell fluid with a convective boundary condition. Ullah et al. [9] reported oscillatory heat transfer and magnetic flux along a magnetically driven cylinder with viscous dissipation and Joule heating. Althobaiti [10] studied activation energy in magnetised dissipative Casson-Maxwell flow through a porous medium with chemical reaction, Joule heating and the Soret effect, and found that it has a strong influence on the flow. Islam et al. [11] applied the Cattaneo-Christov theory to time-dependent MHD Maxwell flow over a stretching cylinder, without porous resistance or Joule heating. Naqvi et al. [12] studied hydromagnetic Casson nanofluid flow over a porous stretching cylinder with Joule heating, viscous dissipation and Newtonian heat and mass conditions, and showed that the magnetic field and Casson parameter reduce the velocity while raising the wall temperature.

Murthy et al. [13] used the Cattaneo-Christov model for mixed convective radiative Casson flow with chemical reaction over a stretching cylinder, and found that reaction and radiation change the flow pattern considerably. Kada et al. [14] derived analytical solutions for radiative, magnetised viscoplastic nanomaterial flow in a cylindrical configuration with Darcy-Forchheimer porosity, Joule heating and chemical reaction. Hayat et al. [15] examined nonlinear convective flow of a Maxwell nanofluid past a stretching cylinder with thermal radiation and chemical reaction, and reported that the Maxwell parameter and curvature parameter significantly influence the velocity and temperature profiles.

Recent studies of nanofluid and non-Newtonian flows have examined thermal radiation, entropy generation and porous-medium resistance. Megahed (2021) [16] examined steady MHD flow of a Maxwell fluid over a stretching sheet embedded in a porous medium under a convective heating condition, and showed that the Maxwell parameter, magnetic field and Eckert number significantly alter the velocity profile and wall heat transfer rate. Hayat and Qasim [17] investigated thermal radiation and Joule heating in MHD Maxwell-fluid flow with thermophoresis. Islam

et al. [18] examined radiative mixed convection of a Maxwell nanofluid over a stretching cylinder with Joule heating, heat source/sink and a convective wall condition, solved by the homotopy analysis method; no porous resistance was included. For viscous fluids, Mukhopadhyay [19] studied MHD slip flow along a stretching cylinder. Mishra and Kumar [20] examined MHD nanofluid flow past a stretching cylinder with velocity and thermal slip, viscous dissipation and Joule heating, and found that the magnetic parameter reduces the velocity while raising the wall temperature; no porous medium or Maxwell constitutive model was used. Ramzan et al. [21] investigated MHD dusty Casson nanofluid flow over a stretching cylinder with Newtonian heating, activation energy and an exothermic chemical reaction, solved by bvp4c, and reported that Newtonian heating raises the temperature for both the fluid and dust phases.

Raj et al. [22] recently studied MHD Maxwell-fluid flow over a stretching cylinder embedded in a porous medium with heat generation and thermal radiation, solved with bvp4c; their energy equation has no viscous dissipation or Joule heating, and the wall temperature is prescribed. Vajravelu et al. [23] analysed axisymmetric MHD flow and heat transfer at a non-isothermal stretching cylinder. Loganathan et al. [24] studied MHD flow of a thermally radiative Maxwell fluid over a heated stretching sheet with Cattaneo–Christov dual diffusion, and found that the Maxwell parameter reduces the fluid velocity while thermal radiation and the Deborah number raise the temperature. Apart from [22], these studies concern viscous, Casson or nanofluid models on disks, sheets or cylinders; none of them treats a Maxwell fluid on a stretching cylinder in a porous medium with combined Joule and Newtonian heating. The Maxwell-fluid studies over flat stretching surfaces [16, 24, 28] omit the cylindrical geometry and porous resistance, and the cylindrical study with Newtonian heating [21] uses a Casson rather than a Maxwell constitutive model.

The wall thermal condition and the constitutive model also matter. Salleh et al. [25] solved boundary-layer flow and heat transfer over a stretching sheet with Newtonian heating, in which the wall heat flux is proportional to the local wall temperature, and Sadeghy et al. [26] analysed the Sakiadis boundary layer of an upper-convected Maxwell fluid. In nanofluid transport, Abbas et al. [27] examined the influence of Darcy–Forchheimer resistance on MHD dissipative non-Newtonian fluid flow in a porous medium with Joule heating effects over an exponentially stretching sheet, reporting that the Forchheimer number and magnetic parameter both reduce the velocity while enhancing the temperature, and Shehzad et al. [28] analysed hydromagnetic steady flow of a Maxwell fluid over a bidirectional stretching surface with prescribed surface temperature and heat flux, showing that the Deborah number retards the velocity and that the local Nusselt and Sherwood numbers are sensitive to the magnetic and Maxwell parameters.

1.1 Novelty and Contribution of the Current Study

The literature reviewed above leaves three gaps. First, the studies that include Joule heating and MHD in Maxwell fluids [5–8] use disks, sheets or wall jets; the cylindrical studies [4, 9, 11, 13, 14, 19, 20] use Newtonian, Casson, nanofluid or viscoplastic models, or omit the porous medium and Newtonian heating; the Maxwell-cylinder study with Joule heating [18] uses a convective wall condition without porous resistance; and the Maxwell-cylinder study in a porous medium [22] has neither Joule heating nor viscous dissipation and uses a prescribed wall temperature. Second, porous-medium resistance has been combined with radiation and chemical reaction in non-Newtonian flows [10, 27], and Newtonian heating has been applied to non-Maxwell cylindrical flows [21], and MHD Maxwell flow over stretching surfaces has been studied without porous resistance [16, 24], but none of these combines porous-medium Darcy resistance with the relaxation-time response of a Maxwell fluid and Newtonian heating over a curved cylindrical surface. Third, the Newtonian (conjugate) heating condition, in which the wall heat flux depends on the local wall temperature [25], has not been explored for Maxwell fluids with Joule heating and porous resistance over a cylinder.

The contributions of the present work are therefore:

(i) a boundary-layer model for axisymmetric flow of an electrically conducting upper-convected Maxwell fluid over a stretching cylinder in a Darcy porous medium, accounting simultaneously for the Lorentz force, Joule heating, viscous dissipation, Newtonian heating and transverse curvature;

(ii) a bvp4c solution of this model, checked against five benchmark studies (maximum deviation 0.032%) and by tolerance, mesh and domain-length tests;

(iii) quantified trends of the skin friction, Nusselt number, wall temperature and Sherwood number with the magnetic, porous, Maxwell, curvature, Prandtl, Eckert, Newtonian heating and Schmidt parameters, with the physical mechanism behind each trend, including the non-monotonic effect of Pr under combined dissipation and Newtonian heating.

These results can guide the use of a magnetic field, porous resistance and fluid elasticity to control wall shear stress and heat and mass transfer rates in polymer processing, coating and chemical-reactor applications.

2 Mathematical Description

Steady, laminar, axisymmetric flow of an incompressible, electrically conducting Maxwell fluid over a stretching cylinder of radius b embedded in a porous medium is considered (Figure 1). The radial and axial coordinates are r_1 and z_1, with corresponding velocity components u_1 and w_1. A magnetic field B_0 is applied normal to the cylinder surface. The resistance of the porous matrix is described by Darcy's law and enters the momentum equation as a linear drag term. The axial momentum equation therefore contains the viscous term, the upper-convected Maxwell relaxation terms with relaxation time λ [8, 11, 15], the Lorentz force modified by fluid elasticity [8], and the Darcy resistance [10, 14].

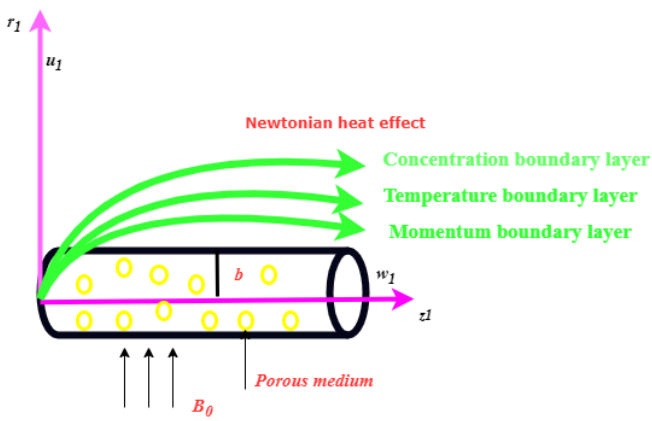

Figure 1. Physical model and coordinate system.

Viscous dissipation and Joule heating are treated as internal heat sources in the energy equation [3, 9, 14]. Merkin's Newtonian heating condition [29] is applied at the wall, so that the surface heat flux is proportional to the surface temperature. The wall concentration is prescribed, and far from the cylinder the velocity, temperature and concentration take their ambient values. With the assumptions of Section 2.1 and the usual boundary-layer approximations, the governing equations take the form of Eqs. (1)-(4), following Wang [30] and Islam et al. [11].

2.1 Basic assumptions

The model rests on the following assumptions:

- The flow is steady, laminar, incompressible and axisymmetric, and the boundary-layer approximations hold.
- The fluid is an upper-convected Maxwell fluid with constant relaxation time λ; density, viscosity, thermal conductivity, specific heat, electrical conductivity and mass diffusivity are constant.
- The cylinder of radius b is stretched axially with a velocity proportional to the axial distance. It is embedded in a homogeneous, isotropic porous medium obeying Darcy's law; Forchheimer (inertial) drag is neglected, and the fluid and solid matrix are in local thermal equilibrium.
- A uniform magnetic field B_0 is applied in the radial direction, normal to the cylinder surface. The magnetic Reynolds number is small, so the induced magnetic field is neglected; there is no external electric field, and Hall and ion-slip effects are neglected.
- The energy equation includes viscous dissipation and Joule heating, but not thermal radiation, internal heat generation or buoyancy.
- The wall heat flux is proportional to the local wall temperature (Newtonian heating), and the wall concentration is fixed [29].
- The species is dilute and chemically inert; Soret and Dufour (cross-diffusion) effects are ignored.
- As $r_1 \to \infty$, the axial velocity vanishes and the temperature and concentration approach their ambient values T_∞ and C_∞.

Equation (1) expresses mass conservation in cylindrical coordinates. On the right-hand side of Eq. (2), the first term represents viscous diffusion, the second the elastic (relaxation) response of the upper-convected Maxwell fluid, the third the Lorentz force due to the applied field B_0 in a fluid of electrical conductivity σ and density ρ, and the last the Darcy resistance of a porous medium of permeability K; ν is the kinematic viscosity. In the energy equation (3),

α_m is the thermal diffusivity, the second term on the right is viscous dissipation (μ is the dynamic viscosity and c_p the specific heat at constant pressure), and the last term is Joule heating. In the species equation (4), C is the concentration and D_B the mass diffusion coefficient. Equations (1)-(4) are adapted from [8, 11, 14, 30].

$$\frac{\partial(r_1 u_1)}{\partial r_1} + \frac{\partial(r_1 w_1)}{\partial z_1} = 0, \tag{1}$$

$$\begin{aligned} u_1 \frac{\partial w_1}{\partial r_1} + w_1 \frac{\partial w_1}{\partial z_1} &= \nu \left(\frac{\partial^2 w_1}{\partial r_1^2} + \frac{1}{r_1}\frac{\partial w_1}{\partial r_1} \right) \\ &- \lambda \left(w_1^2 \frac{\partial^2 w_1}{\partial z_1^2} + u_1^2 \frac{\partial^2 w_1}{\partial r_1^2} \right. \\ &\left. + 2 u_1 w_1 \frac{\partial^2 w_1}{\partial r_1 \partial z_1} \right) \\ &- \frac{\sigma B_0^2}{\rho} \left(w_1 + \lambda u_1 \frac{\partial w_1}{\partial r_1} \right) - \frac{\nu}{K} w_1, \end{aligned} \tag{2}$$

$$\begin{aligned} u_1 \frac{\partial T}{\partial r_1} + w_1 \frac{\partial T}{\partial z_1} &= \alpha_m \left(\frac{\partial^2 T}{\partial r_1^2} + \frac{1}{r_1}\frac{\partial T}{\partial r_1} \right) \\ &+ \frac{\mu}{\rho c_p} \left(\frac{\partial w_1}{\partial r_1} \right)^2 + \frac{\sigma B_0^2}{\rho c_p} w_1^2, \end{aligned} \tag{3}$$

$$u_1 \frac{\partial C}{\partial r_1} + w_1 \frac{\partial C}{\partial z_1} = D_B \left(\frac{\partial^2 C}{\partial r_1^2} + \frac{1}{r_1}\frac{\partial C}{\partial r_1} \right). \tag{4}$$

The boundary conditions are given by Eqs. (5) and (6). At the surface, the stretching velocity is imposed ($u_1 = 0$, $w_1 = w_w = U_0 z_1 / l$, where U_0 is a reference velocity and l a reference length), together with the Newtonian heating condition $\partial T/\partial r_1 = -h_t T$, where the heat transfer coefficient h_t is constant [29], and the prescribed wall concentration $C = C_w$. Far from the cylinder ($r_1 \to \infty$), Eq. (6) requires the axial velocity to vanish and the temperature and concentration to tend to T_∞ and C_∞. These conditions follow [11, 29, 30].

$$\begin{aligned} u_1 = 0, \quad w_1 = w_w = \frac{U_0 z_1}{l}, \\ \frac{\partial T}{\partial r_1} = -h_t T, \quad C = C_w \quad \text{at } r_1 = b, \end{aligned} \tag{5}$$

$$w_1 \to 0, \;\; T \to T_\infty, \;\; C \to C_\infty \quad \text{as } r_1 \to \infty. \tag{6}$$

Introducing the similarity variables and dimensionless quantities of Eq. (12) [11, 30] satisfies the continuity equation (1) identically and transforms Eqs. (2)-(6) into the ordinary differential equations (7)-(9) with boundary conditions (10) and (11). The dimensionless parameters are the curvature parameter α, the Maxwell parameter β, the magnetic parameter M, the porous-medium parameter Po (inversely proportional to the permeability K), the Prandtl number Pr, the Eckert number Ec, the Newtonian heating parameter γ and the Schmidt number Sc. Results expressed in these groups apply to any system with the same parameter values, independently of the units used.

$$\begin{aligned} &(1+2\alpha\eta) g''' + 2\alpha g'' + g g'' - g'^2 + \beta \left(2 g g' g'' - g^2 g''' \right) \\ &\quad - \frac{\alpha\beta}{1+2\alpha\eta} g^2 g'' - M \left(g' - \beta g g'' \right) - Po\, g' = 0, \end{aligned} \tag{7}$$

$$\begin{aligned} &(1+2\alpha\eta)\theta'' + 2\alpha\theta' + Pr\, g \theta' \\ &\quad + Pr\, Ec \left[(1+2\alpha\eta) g''^2 + M g'^2 \right] = 0, \end{aligned} \tag{8}$$

$$(1+2\alpha\eta)\phi'' + 2\alpha\phi' + Sc\, g \phi' = 0. \tag{9}$$

The dimensionless boundary conditions are

$$\begin{aligned} g(0) = 0, \quad g'(0) = 1, \\ \theta'(0) = -\gamma \left[1 + \theta(0) \right], \quad \phi(0) = 1, \end{aligned} \tag{10}$$

$$g'(\infty) = 0, \;\; \theta(\infty) = 0, \;\; \phi(\infty) = 0, \tag{11}$$

where the similarity variables and dimensionless groups are

$$\begin{aligned} \eta &= \sqrt{\frac{U_0}{\nu l}} \frac{r_1^2 - b^2}{2b}, \quad w_1 = \frac{U_0 z_1}{l} g'(\eta), \\ u_1 &= -\frac{b}{r_1} \sqrt{\frac{U_0 \nu}{l}}\, g(\eta), \quad \theta(\eta) = \frac{T - T_\infty}{T_\infty}, \\ \phi(\eta) &= \frac{C - C_\infty}{C_w - C_\infty}, \quad \alpha = \frac{1}{b}\sqrt{\frac{\nu l}{U_0}}, \quad \beta = \frac{\lambda U_0}{l}, \\ M &= \frac{\sigma B_0^2 l}{\rho U_0}, \quad Po = \frac{\nu l}{K U_0}, \quad Pr = \frac{\nu}{\alpha_m}, \\ Ec &= \frac{w_w^2}{c_p T_\infty}, \quad \gamma = h_t \sqrt{\frac{\nu l}{U_0}}, \quad Sc = \frac{\nu}{D_B}. \end{aligned} \tag{12}$$

The engineering quantities of interest are the skin-friction coefficient, the local Sherwood number and the local Nusselt number, defined in Eqs. (13)-(15) [11, 14]. The skin-friction coefficient measures the wall shear stress and hence the drag and power needed to stretch the cylinder. The Nusselt number measures the wall heat transfer rate; with the Newtonian heating condition (10) it is proportional to $1+\theta(0)$ and therefore increases with the dimensionless wall temperature. The Sherwood number represents

the wall mass transfer rate that matters in chemical reactors, separation processes and coating operations.

$$C_f = \frac{\tau_w}{\rho w_w^2}, \quad \tau_w = \mu \left(\frac{\partial w_1}{\partial r_1}\right)_{r_1=b}, \qquad (13)$$
$$C_f\, Re_z^{1/2} = g''(0),$$

$$Sh_z = \frac{z_1 j_w}{D_B(C_w - C_\infty)}, \quad j_w = -D_B \left(\frac{\partial C}{\partial r_1}\right)_{r_1=b},$$
$$Sh_z\, Re_z^{-1/2} = -\phi'(0), \qquad (14)$$

$$Nu_z = \frac{z_1 q_w}{kT_\infty}, \quad q_w = -k \left(\frac{\partial T}{\partial r_1}\right)_{r_1=b}, \qquad (15)$$
$$Nu_z\, Re_z^{-1/2} = -\theta'(0) = \gamma\left[1 + \theta(0)\right],$$

where $Re_z = w_w z_1/\nu$ is the local Reynolds number and k the thermal conductivity.

3 Solution Method

The boundary value problem (7)-(11) is strongly nonlinear and has no exact solution, so it is solved in MATLAB with bvp4c [31]. This finite-difference code implements the three-stage Lobatto IIIa collocation formula; it returns a C^1-continuous solution that is fourth-order accurate on the mesh, adapts the mesh automatically and controls the residual of the continuous solution.

The higher-order equations are rewritten as a first-order system with the variables $a_1, \ldots, a_7$, where $a_1 = g$, $a_2 = g'$, $a_3 = g''$, $a_4 = \theta$, $a_5 = \theta'$, $a_6 = \phi$ and $a_7 = \phi'$, giving Eqs. (16)-(18). The relative tolerance is set to 10^{-8} and the infinite domain is truncated at $\eta_\infty = 30$. Because the curvature term makes the temperature and concentration decay algebraically rather than exponentially, these fields need a much longer domain than the velocity field (Section 4). The initial guesses satisfy the boundary conditions, and parameter sweeps use the previous solution as the initial guess. Unless stated otherwise, the reference values are $\beta = 0.1$, $M = 0.2$, $\alpha = 0.1$, $Po = 0.2$, $Pr = 1.0$, $Ec = 0.2$, $\gamma = 0.1$ and $Sc = 1.0$; in each table row and figure only the indicated parameter is changed.

$$a_1' = a_2, \quad a_2' = a_3, \quad a_3' = \frac{N}{1 + 2\alpha\eta - \beta a_1^2},$$
$$N = a_2^2 - a_1 a_3 - 2\alpha a_3 - 2\beta a_1 a_2 a_3 + \frac{\alpha\beta\, a_1^2 a_3}{1 + 2\alpha\eta} \qquad (16)$$
$$+ M(a_2 - \beta a_1 a_3) + Po\, a_2,$$
$$a_4' = a_5, \quad a_5' = -\frac{2\alpha a_5 + Pr\, a_1 a_5 + Pr\, Ec\, Q}{1 + 2\alpha\eta},$$
$$Q = (1 + 2\alpha\eta) a_3^2 + M a_2^2, \qquad (17)$$
$$a_6' = a_7, \quad a_7' = -\frac{(2\alpha + Sc\, a_1) a_7}{1 + 2\alpha\eta}, \qquad (18)$$

with $a_1(0) = 0$, $a_2(0) = 1$, $a_5(0) + \gamma[1 + a_4(0)] = 0$, $a_6(0) = 1$, and $a_2(\eta_\infty) = a_4(\eta_\infty) = a_6(\eta_\infty) = 0$.

4 Validation of the Present Work

The classical problem of upper-convected Maxwell flow over a linearly stretching sheet [32–35] is recovered from the present model in the limit $\alpha = M = Po = 0$. Table 1 compares the present skin-friction coefficients $-g''(0)$ with those of Subhas Abel et al. [32], Megahed (2013) [33], Waqas et al. [34], Irfan et al. [35] and Ahmed et al. [36]; the Oldroyd-B results of [34, 35] are taken with zero retardation time, for which the model reduces to the Maxwell fluid. For $\beta = 0$ (Newtonian fluid) every study gives $-g''(0) = 1$, the exact value for a linearly stretching sheet. The present results agree with Irfan et al. [35] to within 3×10^{-6} and with all five references to within 0.032%. At $\beta = 1.0$, where only Ahmed et al. [36] report a value, the present result is 1.241753 against 1.241722, a difference of 0.003%. The skin-friction coefficient increases with β because larger elastic stresses in the Maxwell fluid raise the wall shear stress.

4.1 Convergence and accuracy of the numerical solution

Besides the benchmark comparison, the solution was checked in three ways for the reference case (first row of Table 4), monitoring $-g''(0)$, $-\theta'(0)$ and $-\phi'(0)$.

- *Tolerance independence.* The relative tolerance was reduced from 10^{-3} to 10^{-10} (Table 2). For tolerances of 10^{-6} and smaller, the three wall quantities agree to eight decimal places, and in every case the maximum residual of the collocation solution is below the prescribed tolerance. A tolerance of 10^{-8} is used for all results.
- *Mesh independence.* Because the solver adapts the mesh, the converged solution should not depend

Table 1. Comparison of the skin-friction coefficient $-g''(0)$ with published results for different values of β ($\alpha = M = Po = 0$).

β	Ref. [32]	Ref. [33]	Ref. [34]	Ref. [35]	Ref. [36]	Present
0.0	1.000000	0.999978	1.000000	1.0000000	1.000000	1.00000000
0.2	1.051948	1.051945	1.051889	1.0518890	1.051556	1.05188903
0.4	1.101850	1.101848	1.101903	1.1019035	1.101603	1.10190275
0.6	1.150163	1.150160	1.150137	1.1501374	1.150356	1.15013508
0.8	1.196692	1.196690	1.196711	1.1967114	1.196711	1.19671233
1.0	-	-	-	-	1.241722	1.24175324
1.2	1.285257	1.285253	1.285363	1.2853630	1.285355	1.28536641

Table 2. Effect of the relative tolerance on the wall quantities (reference case, $\eta_\infty = 30$).

Rel. tolerance	$-g''(0)$	$-\theta'(0)$	$-\phi'(0)$	Max. residual
10^{-3}	1.24874576	0.14918462	0.56035758	6.37×10^{-6}
10^{-4}	1.24874744	0.14919232	0.56034109	2.61×10^{-6}
10^{-6}	1.24874761	0.14919355	0.56033950	9.81×10^{-7}
10^{-8}	1.24874761	0.14919355	0.56033950	9.98×10^{-9}
10^{-10}	1.24874761	0.14919355	0.56033950	9.99×10^{-11}

Table 3. Effect of the domain length η_∞ on the wall quantities (reference case, tolerance 10^{-8}).

η_∞	$-g''(0)$	$-\theta'(0)$	$-\phi'(0)$	$g''(\eta_\infty)$
5	1.24973367	0.14512026	0.59682099	-8.14×10^{-3}
10	1.24875797	0.14849451	0.56612552	-2.34×10^{-4}
15	1.24874787	0.14900800	0.56185971	-1.53×10^{-5}
20	1.24874762	0.14913485	0.56081931	-1.57×10^{-6}
25	1.24874761	0.14917678	0.56047649	-2.17×10^{-7}
30	1.24874761	0.14919355	0.56033950	-3.71×10^{-8}
40	1.24874761	0.14920511	0.56024517	-1.69×10^{-9}

on the initial mesh. Initial meshes of 20, 50, 100, 200 and 400 uniformly spaced points all gave $-g''(0) = 1.24874761$, $-\theta'(0) = 0.14919355$ and $-\phi'(0) = 0.56033950$.

- *Domain-length independence.* Table 3 shows that $-g''(0)$ is already converged at $\eta_\infty = 10$ (change below 0.001% up to $\eta_\infty = 40$), but $-\theta'(0)$ and $-\phi'(0)$ still change by 0.43% and 0.94% between $\eta_\infty = 10$ and 20. For large η, $g \to g_\infty$ and Eqs. (8) and (9) give $\theta', \phi' \propto (1 + 2\alpha\eta)^{-1-Pr\, g_\infty/(2\alpha)}$ and $(1 + 2\alpha\eta)^{-1-Sc\, g_\infty/(2\alpha)}$, so the temperature and concentration decay algebraically rather than exponentially. Between $\eta_\infty = 30$ and 40 the changes fall to 0.008% and 0.017%, and $\eta_\infty = 30$ is therefore adopted.

Together with Table 1, these tests support the accuracy and convergence of the reported results.

5 Results and Discussion

Figure 2 shows the effect of the magnetic parameter M on the temperature profile $\theta(\eta)$, where η is the dimensionless distance from the cylinder surface. As M increases from 0 to 2, the wall temperature $\theta(0)$ rises from 0.421 to 1.100 and the thermal boundary layer thickens. The transverse magnetic field produces a Lorentz force that opposes the flow, slows the fluid near the wall and reduces convective heat removal. The work done against the Lorentz force is also dissipated as Joule heat (the term $Pr\, Ec\, M g'^2$ in Eq. (8)), which acts as an internal heat source. Both mechanisms raise the fluid temperature, and because the wall is subject to Newtonian heating, the higher wall temperature also increases the wall heat flux: the Nusselt number rises by 10.61% between $M = 0.5$ and 1.0 (Table 4).

According to Figure 3, the concentration $\phi(\eta)$ increases and the concentration boundary layer thickens as M increases; at $\eta = 2$, ϕ grows from 0.271 ($M = 0$)

Table 4. Skin-friction coefficient, Nusselt number and wall temperature for different values of the governing parameters. Reference values: $\beta = 0.1$, $M = 0.2$, $\alpha = 0.1$, $Po = 0.2$, $Pr = 1.0$, $Ec = 0.2$, $\gamma = 0.1$, $Sc = 1.0$, $\eta_\infty = 30$; only the listed parameter is changed.

Parameter	Value	$-g''(0)$	$-\theta'(0)$	$\theta(0)$
β	0.1	1.24874761	0.14919355	0.491936
	0.2	1.27244837	0.15070472	0.507047
	0.3	1.29585952	0.15223349	0.522335
α	0.1	1.24874761	0.14919355	0.491936
	0.2	1.28875626	0.14787054	0.478705
	0.3	1.32803768	0.14639702	0.463970
M	0.5	1.37275462	0.15958029	0.595803
	0.8	1.48579044	0.16977305	0.697730
	1	1.55635083	0.17650971	0.765097
Po	0.3	1.29010620	0.15102877	0.510288
	0.4	1.33007926	0.15285542	0.528554
	0.5	1.36880396	0.15467550	0.546755
Pr	2	-	0.14228962	0.422896
	3	-	0.14143775	0.414377
	4	-	0.14174172	0.417417
Ec	0.3	-	0.16292878	0.629288
	0.4	-	0.17666401	0.766640
	0.5	-	0.19039924	0.903992
γ	0.1	-	0.14919355	0.491936
	0.2	-	0.38119432	0.905972
	0.3	-	0.79142450	1.638082

"-": equal to the reference value 1.24874761, since Pr, Ec and γ do not enter Eq. (7).

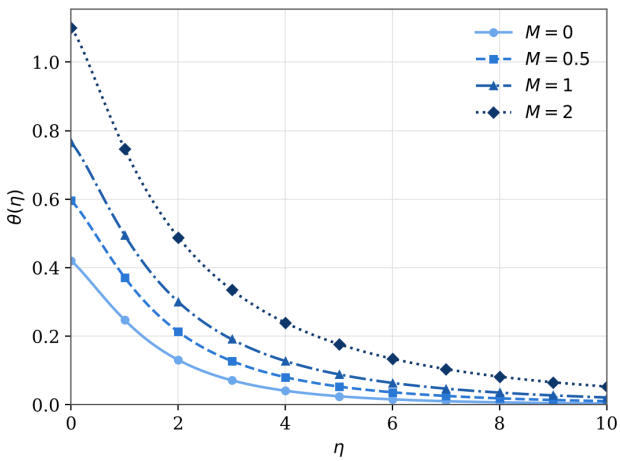

Figure 2. Temperature profile $\theta(\eta)$ for different values of the magnetic parameter M ($\beta = 0.1$, $\alpha = 0.1$, $Po = 0.2$, $Pr = 1$, $Ec = 0.2$, $\gamma = 0.1$).

to 0.412 ($M = 2$). The Lorentz force lowers the fluid velocity, so less solute is carried away from the surface by the inward radial flow and the concentration gradient at the wall decreases. Consistently, the Sherwood number falls from 0.581 to 0.445 over the same range of M.

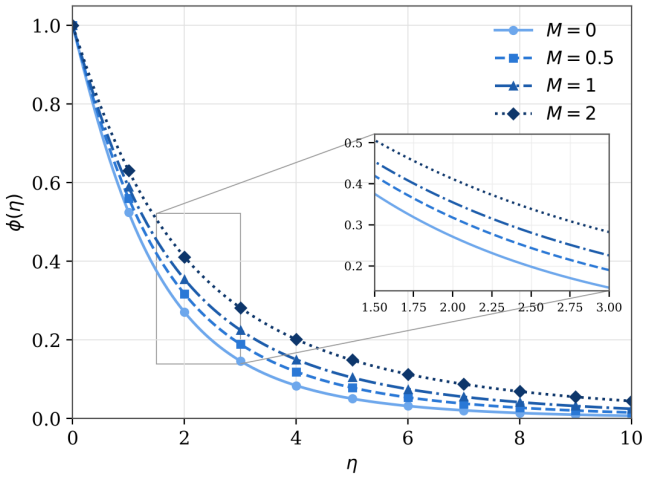

Figure 3. Concentration profile $\phi(\eta)$ for different values of M ($\beta = 0.1$, $\alpha = 0.1$, $Po = 0.2$, $Sc = 1$); the inset enlarges $1.5 \le \eta \le 3$.

Figure 4 shows the effect of the porous-medium parameter Po on the temperature profile. $Po = 0$ corresponds to a clear fluid; larger Po means a less permeable medium, since Po is inversely proportional to K. As Po increases from 0 to 1, $\theta(0)$ rises from 0.455 to 0.637 and the thermal boundary layer thickens. Darcy drag reduces the fluid velocity near the surface and with it the convective transport of heat away from the wall, while the steeper velocity gradient at the stretching wall (Table 4) increases viscous heating.

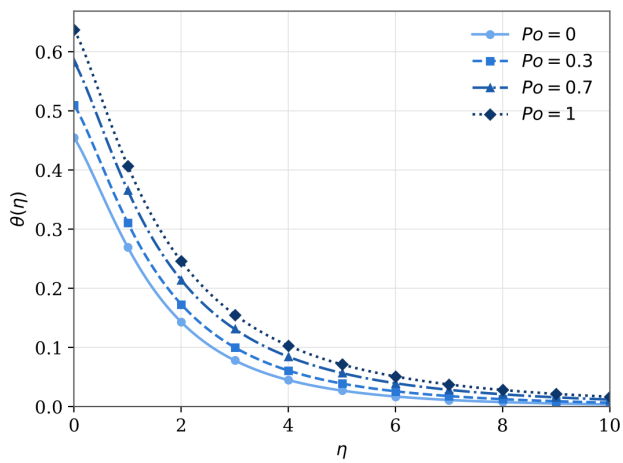

Figure 4. Temperature profile $\theta(\eta)$ for different values of the porous-medium parameter Po ($\beta = 0.1$, $M = 0.2$, $\alpha = 0.1$, $Pr = 1$, $Ec = 0.2$, $\gamma = 0.1$).

As shown in Figure 5, the concentration profile also rises as Po increases from 0 to 1, and the Sherwood number decreases from 0.579 to 0.501. The resistance of the porous matrix slows the flow, thickening the concentration boundary layer and reducing convective

transport of solute. Po affects the concentration field less than the temperature field because the species equation has no source term comparable to viscous dissipation or Joule heating.

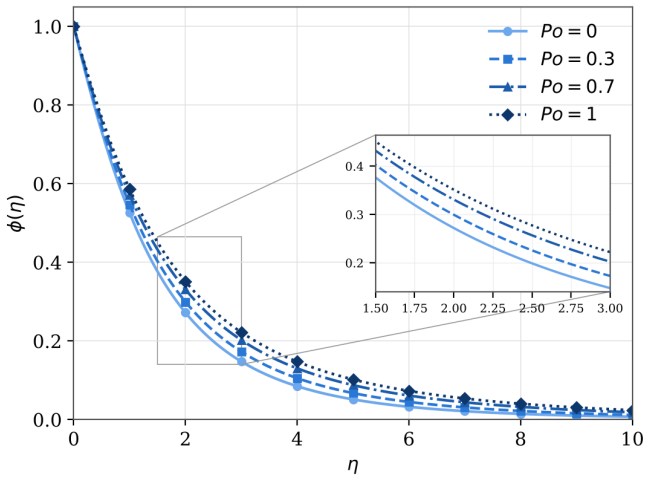

Figure 5. Concentration profile $\phi(\eta)$ for different values of the porous-medium parameter Po ($\beta = 0.1$, $M = 0.2$, $\alpha = 0.1$, $Sc = 1$); the inset enlarges $1.5 \leq \eta \leq 3$.

Figure 6 shows the influence of the Maxwell parameter β on the temperature profile; $\beta = 0$ corresponds to a Newtonian (viscous) fluid. As β increases from 0 to 0.6, $\theta(0)$ rises from 0.477 to 0.569 and the thermal boundary layer thickens. A longer relaxation time, measured by β, makes the near-wall fluid respond more slowly to the imposed stretching. The reduced convective transport, together with the higher wall shear stress (3.77% for $\beta = 0.1 \rightarrow 0.3$, Table 4) and hence stronger viscous dissipation, raises the fluid temperature.

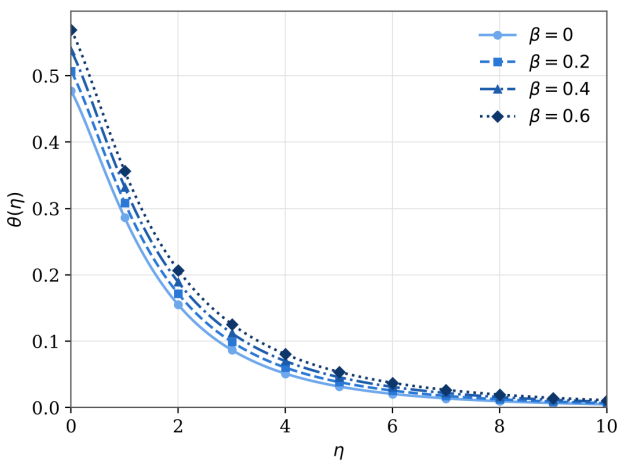

Figure 6. Temperature profile $\theta(\eta)$ for different values of the Maxwell parameter β ($M = 0.2$, $\alpha = 0.1$, $Po = 0.2$, $Pr = 1$, $Ec = 0.2$, $\gamma = 0.1$).

Figure 7 shows that the concentration profile rises and the concentration boundary layer thickens as β increases from 0 to 0.6, while the Sherwood number decreases from 0.568 to 0.526. The elastic retardation of the flow reduces convective removal of the species, which then leaves the wall region more slowly.

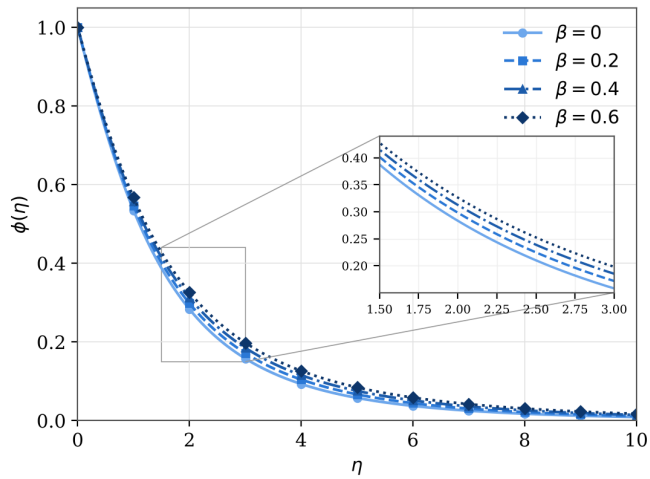

Figure 7. Concentration profile $\phi(\eta)$ for different values of the Maxwell parameter β ($M = 0.2$, $\alpha = 0.1$, $Po = 0.2$, $Sc = 1$); the inset enlarges $1.5 \leq \eta \leq 3$.

Figure 8 shows the effect of the curvature parameter α on the temperature distribution. The profiles cross at $\eta \approx 1.25$. Close to the wall the temperature decreases with α ($\theta(0)$ falls from 0.492 at $\alpha = 0.1$ to 0.449 at $\alpha = 0.4$), whereas further out it increases and the thermal boundary layer becomes thicker. A larger α corresponds to a thinner cylinder. The extra radial-spreading term $2\alpha\theta'$ in Eq. (8) and the stronger near-wall shear (the skin friction rises by 6.35% from $\alpha = 0.1$ to 0.3) remove heat from the wall region more effectively, which lowers the wall temperature under Newtonian heating. The same spreading carries heat further from the surface, so the outer part of the layer is warmer and decays more slowly.

Figure 9 shows a similar pattern for the concentration: the profiles cross near $\eta \approx 0.59$, inside which ϕ falls more steeply for larger α, and beyond which the concentration is higher and the boundary layer thicker. The steeper wall gradient raises the Sherwood number by 9.21% when α increases from 0.1 to 0.3 (Table 5).

Table 4 lists the skin-friction coefficient, the Nusselt number and the wall temperature for various values of the governing parameters. Under Newtonian heating, any parameter that raises the wall temperature also raises the Nusselt number, since $-\theta'(0) = \gamma[1 + \theta(0)]$. Increasing β from 0.1 to 0.3 raises the skin friction from 1.24875 to 1.29586 (3.77%) and the Nusselt number from 0.14919 to 0.15223 (2.04%): elastic

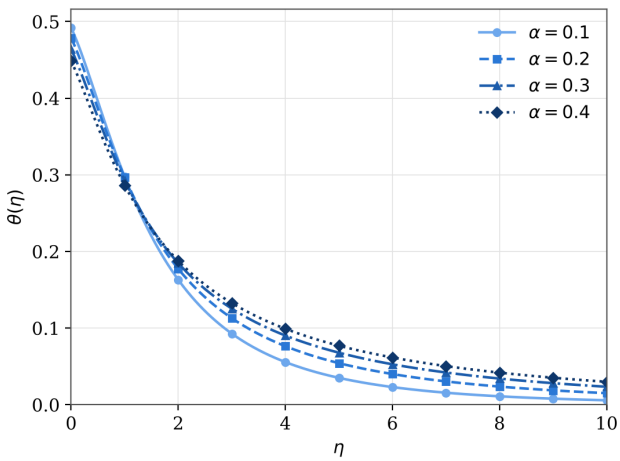

Figure 8. Temperature profile $\theta(\eta)$ for different values of the curvature parameter α ($\beta = 0.1$, $M = 0.2$, $Po = 0.2$, $Pr = 1$, $Ec = 0.2$, $\gamma = 0.1$).

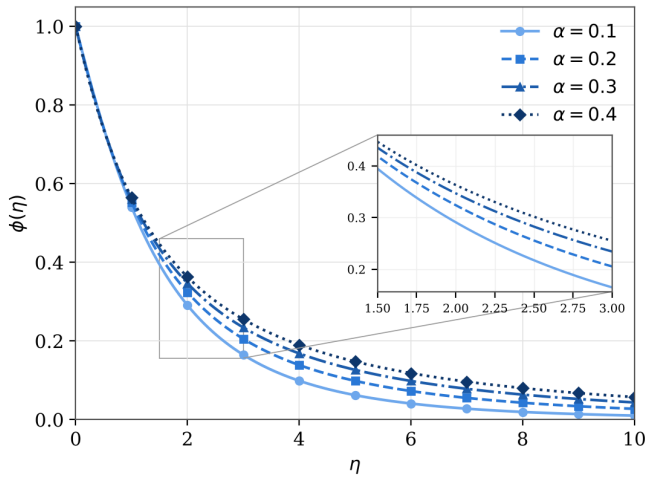

Figure 9. Concentration profile $\phi(\eta)$ for different values of the curvature parameter α ($\beta = 0.1$, $M = 0.2$, $Po = 0.2$, $Sc = 1$); the inset enlarges $1.5 \leq \eta \leq 3$.

stresses increase the wall shear, and the accompanying retardation of the flow raises the wall temperature. Increasing α from 0.1 to 0.3 raises the skin friction by 6.35% but lowers the Nusselt number by 1.87%, in line with the lower wall temperature seen in Figure 8.

Increasing M from 0.5 to 1.0 raises the skin friction by 13.37% (from 1.37275 to 1.55635) and the Nusselt number by 10.61% (from 0.15958 to 0.17651). Joule heating raises the wall temperature, and the Lorentz force steepens the near-wall velocity gradient of the stretching flow, which increases the wall shear. Likewise, increasing Po from 0.3 to 0.5 raises the skin friction by 6.10% and the Nusselt number by 2.41%, because Darcy drag acts in the same direction as the Lorentz force; the Darcy term, unlike the magnetic one, adds no heat source, so its thermal effect is smaller. The Nusselt number varies non-monotonically with Pr: it falls from 0.14919 at $Pr = 1$ to a minimum of about 0.1414 near $Pr = 3$ and then rises slightly (0.14174 at $Pr = 4$). A larger Pr strengthens convection (the term $Pr\, g\theta'$), which thins the thermal boundary layer and lowers the wall temperature, but it also strengthens the dissipative sources, which scale with $Pr\, Ec$. The first effect dominates at small Pr and the second beyond $Pr \approx 3$. Increasing Ec from 0.3 to 0.5 raises the Nusselt number by 16.86% (from 0.16293 to 0.19040); since Eq. (8) is linear in θ, the wall temperature increases linearly with Ec.

Heat transfer is most sensitive to the Newtonian heating parameter: increasing γ from 0.1 to 0.3 raises the Nusselt number from 0.14919 to 0.79142, a factor of about 5.3, and the wall temperature from 0.492 to 1.638. A larger γ (a higher heat transfer coefficient h_t) couples the wall heat flux more strongly to the wall temperature, so both increase. Pr, Ec and γ appear only in the energy equation and therefore do not affect the skin friction.

Table 5 gives the Sherwood number. It decreases by 2.57%, 6.73% and 2.92% when β, M and Po increase from 0.1 to 0.3, 0.5 to 1.0 and 0.3 to 0.5, respectively, consistent with the thicker concentration boundary layers in Figures 3, 5 and 7; all three parameters weaken the flow that convects solute away from the wall. Curvature has the opposite effect: the Sherwood number rises by 9.21% when α increases from 0.1 to 0.3. The Schmidt number dominates mass transfer: as Sc increases from 2 to 4, the Sherwood number rises from 0.89097 to 1.36129 (52.79%), because a lower mass diffusivity thins the concentration boundary layer and steepens the wall gradient. Because the species equation is coupled to the flow only through g, Pr, Ec and γ have no effect on the Sherwood number. Within the parameter range studied, mass transfer is therefore controlled mainly by Sc and α, whereas the magnetic, porous and viscoelastic parameters act mainly on the momentum and thermal fields. This distinction is useful for chemical reactors, pollutant dispersion and separation processes in porous media.

The porous-medium parameter deserves a final remark. Because Po is inversely proportional to K, the Darcy term $-Po\, g'$ in Eq. (7) acts as a distributed body force opposing the motion. It decelerates the boundary-layer fluid and steepens the velocity profile at the stretching wall, which increases the wall shear stress by 6.10% for $Po = 0.3$-0.5 (Table 4). Under Newtonian heating, the resulting rise in wall

Table 5. Sherwood number $-\phi'(0)$ for different values of the governing parameters.

Parameter	Value	$-\phi'(0)$
β	0.1	0.56033950
	0.2	0.55303445
	0.3	0.54593297
α	0.1	0.56033950
	0.2	0.58496496
	0.3	0.61194661
M	0.5	0.53412098
	0.8	0.51158053
	1	0.49817335
Po	0.3	0.55162865
	0.4	0.54336505
	0.5	0.53550522
Sc	2	0.89097413
	3	1.14618416
	4	1.36128682

temperature increases the heat flux (Nusselt number $+2.41\%$), while the Sherwood number decreases by 2.92%. In practice, lowering the permeability of the porous medium raises the wall heat flux under conjugate heating, at the cost of higher wall shear stress and slightly lower mass transfer.

6 Conclusions

This study analysed steady axisymmetric flow, heat transfer and mass transfer of an electrically conducting Maxwell fluid over a stretching cylinder in a Darcy porous medium with Joule heating, viscous dissipation and Newtonian heating. Similarity transformations reduced the governing equations to nonlinear ordinary differential equations, which were solved with a fourth-order collocation method (bvp4c). The solution agrees with five published benchmarks to within 0.032%, and tolerance, mesh and domain-length tests confirmed its convergence; the temperature and concentration fields require a domain of $\eta_\infty \approx 30$ because they decay algebraically. The main conclusions are:

- Increasing the magnetic parameter M from 0.5 to 1.0 raises the skin-friction coefficient by 13.37% and the Nusselt number by 10.61% and lowers the Sherwood number by 6.73%; the Lorentz force and Joule heating raise the temperature and concentration profiles.
- Increasing the porous-medium parameter Po from 0.3 to 0.5 raises the skin friction and Nusselt number by 6.10% and 2.41% and lowers the Sherwood number by 2.92%; Darcy drag thickens the thermal and concentration boundary layers.
- Increasing the Maxwell parameter β from 0.1 to 0.3 raises the skin friction by 3.77% and the Nusselt number by 2.04% and lowers the Sherwood number by 2.57%, reflecting the retarding effect of fluid elasticity.
- A larger curvature parameter lowers the wall temperature but thickens the outer thermal and concentration layers; from $\alpha = 0.1$ to 0.3 the skin friction and Sherwood number rise by 6.35% and 9.21%, while the Nusselt number falls by 1.87%.
- The Nusselt number increases by 16.86% when the Eckert number rises from 0.3 to 0.5 and varies non-monotonically with the Prandtl number, with a minimum near $Pr \approx 3$.
- The Newtonian heating parameter has the largest effect on heat transfer: increasing γ from 0.1 to 0.3 raises the Nusselt number from 0.1492 to 0.7914, about 5.3 times.
- Increasing the Schmidt number from 2 to 4 raises the Sherwood number by 52.79%.

Future work could include entropy-generation analysis, unsteady flow, Darcy-Forchheimer inertia, thermal radiation and variable fluid properties.

Data Availability Statement

The data supporting the findings of this study are available from the corresponding author upon reasonable request.

Funding

This work was supported without any funding.

Conflicts of Interest

The author declares no conflicts of interest.

AI Use Statement

The author declares that no generative AI was used in the preparation of this manuscript.

Ethical Approval and Consent to Participate

Not applicable. This work did not involve human participants, animals, or personal or sensitive data.

References

[1] Khan, S. A., Khan, M. I., Alsallami, S. A., Alhazmi, S. E., Alharbi, F. M., & El-Zahar, E. R. (2022). Irreversibility analysis in hydromagnetic flow of Newtonian fluid with Joule heating: Darcy-Forchheimer model. *Journal of Petroleum Science and Engineering, 212*, 110206. [CrossRef]

[2] Sudarmozhi, K., Iranian, D., Khan, I., Ashmaig, M. A. M., & Omer, A. S. (2023). Thermofluid of Maxwellian type past a porous stretching cylinder with heat generation and chemical reaction. *International Journal of Thermofluids, 20*, 100444. [CrossRef]

[3] Mahanthesh, B., Al-Kouz, W., Swain, K., & Rout, P. K. (2021). Computational modeling of heat transfer in magneto-non-Newtonian material in a circular tube with viscous and Joule heating. *Heat Transfer, 50*(7), 6703-6718. [CrossRef]

[4] Khedher, N. B., Ullah, Z., Alturki, M., Mirza, C. R., & Eldin, S. M. (2024). Effect of Joule heating and MHD on periodical analysis of current density and amplitude of heat transfer of electrically conducting fluid along thermally magnetized cylinder. *Ain Shams Engineering Journal, 15*(2), 102374. [CrossRef]

[5] Ahmed, J., Khan, M., & Ahmad, L. (2019). Joule heating effects in thermally radiative swirling flow of Maxwell fluid over a porous rotating disk. *International Journal of Thermophysics, 40*(12), 106. [CrossRef]

[6] Gangadhar, K., Edukondala Nayak, R., Vinodh Kumar, P., & Chamkha, A. J. (2026). Von Kármán viscous pump of rotating disk in a magnetized Maxwell fluid with Joule heating. *Waves in Random and Complex Media, 36*(4), 6386-6405. [CrossRef]

[7] Suraiah Palaiah, S., Basha, H., Reddy, G. J., & Sheremet, M. A. (2021). Magnetized dissipative Soret effect on chemically reactive Maxwell fluid over a stretching sheet with Joule heating. *Coatings, 11*(5), 528. [CrossRef]

[8] Zaidi, Z. A., & Mohyud-Din, S. T. (2017). Effect of joule heating and MHD in the presence of convective boundary condition for upper convected Maxwell fluid through wall jet. *Journal of Molecular Liquids, 230*, 230-234. [CrossRef]

[9] Ullah, Z., Aldhabani, M. S., & Qaiser, M. A. (2023). Oscillatory and periodical behavior of heat transfer and magnetic flux along magnetic-driven cylinder with viscous dissipation and Joule heating effects. *Mathematics, 11*(18), 3917. [CrossRef]

[10] Althobaiti, N. (2024). Importance of activation energy on magnetized dissipative Casson-Maxwell fluid through porous medium incorporating chemical reaction, Joule heating, and Soret effects: Numerical study. *Journal of Applied Mathematics, 2024*(1), 5730530. [CrossRef]

[11] Islam, S., Dawar, A., Shah, Z., & Tariq, A. (2021). Cattaneo–Christov theory for a time-dependent magnetohydrodynamic Maxwell fluid flow through a stretching cylinder. *Advances in Mechanical Engineering, 13*(7), 16878140211030152. [CrossRef]

[12] Naqvi, S. M. R. S., Muhammad, T., & Asma, M. (2020). Hydromagnetic flow of Casson nanofluid over a porous stretching cylinder with Newtonian heat and mass conditions. *Physica A: Statistical Mechanics and its Applications, 550*, 123988. [CrossRef]

[13] Murthy, D. V., Babu, P. S., & Srinivasulu, C. (2023). Cattaneo-Christov model for mixed convective radiative flow of Casson fluid with Joule heating in the presence of chemical reaction over a stretching cylinder. *JP Journal of Heat and Mass Transfer, 34*, 153-181. [CrossRef]

[14] Kada, B., Bilal, S., Pasha, A. A., Waqas, M., Zamri, N., & Formanova, S. B. (2024). Analytical assessment based on radiative-magnetized nanomaterial viscoplastic flow configured by cylindrical regime with Darcy–Forchheimer porosity, Joule heating and chemical reaction. *Case Studies in Thermal Engineering, 61*, 104960. [CrossRef]

[15] Hayat, T., Rashid, M., Alsaedi, A., & Asghar, S. (2019). Nonlinear convective flow of Maxwell nanofluid past a stretching cylinder with thermal radiation and chemical reaction. *Journal of the Brazilian Society of Mechanical Sciences and Engineering, 41*(2), 86. [CrossRef]

[16] Megahed, A. M. (2021). Improvement of heat transfer mechanism through a Maxwell fluid flow over a stretching sheet embedded in a porous medium and convectively heated. *Mathematics and Computers in Simulation, 187*, 97-109. [CrossRef]

[17] Hayat, T., & Qasim, M. (2010). Influence of thermal radiation and Joule heating on MHD flow of a Maxwell fluid in the presence of thermophoresis. *International Journal of Heat and Mass Transfer, 53*(21-22), 4780-4788. [CrossRef]

[18] Islam, S., Khan, A., Kumam, P., Alrabaiah, H., Shah, Z., Khan, W., ... & Jawad, M. (2020). Radiative mixed convection flow of Maxwell nanofluid over a stretching cylinder with Joule heating and heat source/sink effects. *Scientific Reports, 10*, 17823. [CrossRef]

[19] Mukhopadhyay, S. (2013). MHD boundary layer slip flow along a stretching cylinder. *Ain Shams Engineering Journal, 4*(2), 317-324. [CrossRef]

[20] Mishra, A., & Kumar, M. (2020). Velocity and thermal slip effects on MHD nanofluid flow past a stretching cylinder with viscous dissipation and Joule heating. *SN Applied Sciences, 2*(8), 1350. [CrossRef]

[21] Ramzan, M., Shaheen, N., Chung, J. D., Kadry, S., Chu, Y. M., & Howari, F. (2021). Impact of Newtonian heating and Fourier and Fick's laws on a magnetohydrodynamic dusty Casson nanofluid flow with variable heat source/sink over a stretching cylinder. *Scientific Reports, 11*(1), 2357. [CrossRef]

[22] Raj, U., Sagadevan, P., & Alessa, N. (2024). Effect of heat generation on MHD Maxwell fluid flow on a

stretching cylinder embedded in a porous medium along with impact of radiation. *Journal of King Saud University - Science*, 36, 103530. [CrossRef]

[23] Vajravelu, K., Prasad, K. V., & Santhi, S. R. (2012). Axisymmetric magneto-hydrodynamic (MHD) flow and heat transfer at a non-isothermal stretching cylinder. *Applied Mathematics and computation, 219*(8), 3993-4005. [CrossRef]

[24] Loganathan, K., Alessa, N., Namgyel, N., & Karthik, T. S. (2021). MHD flow of thermally radiative Maxwell fluid past a heated stretching sheet with Cattaneo–Christov dual diffusion. *Journal of Mathematics, 2021*(1), 5562667. [CrossRef]

[25] Salleh, M. Z., Nazar, R., & Pop, I. (2010). Boundary layer flow and heat transfer over a stretching sheet with Newtonian heating. *Journal of the Taiwan Institute of Chemical Engineers, 41*(6), 651-655. [CrossRef]

[26] Sadeghy, K., Najafi, A. H., & Saffaripour, M. (2005). Sakiadis flow of an upper-convected Maxwell fluid. *International Journal of Non-Linear Mechanics, 40*(9), 1220-1228. [CrossRef]

[27] Abbas, A., Jeelani, M. B., & Alharthi, N. H. (2022). Darcy–Forchheimer relation influence on MHD dissipative third-grade fluid flow and heat transfer in porous medium with joule heating effects: A numerical approach. *Processes, 10*(5), 906. [CrossRef]

[28] Shehzad, S. A., Alsaedi, A., & Hayat, T. (2013). Hydromagnetic steady flow of Maxwell fluid over a bidirectional stretching surface with prescribed surface temperature and prescribed surface heat flux. *Plos One, 8*(7), e68139. [CrossRef]

[29] Merkin, J. H. (1994). Natural-convection boundary-layer flow on a vertical surface with Newtonian heating. *International Journal of Heat and Fluid Flow, 15*(5), 392-398. [CrossRef]

[30] Wang, C. Y. (1988). Fluid flow due to a stretching cylinder. *The Physics of Fluids, 31*(3), 466-468. [CrossRef]

[31] Kierzenka, J., & Shampine, L. F. (2001). A BVP solver based on residual control and the Maltab PSE. *ACM Transactions on Mathematical Software (TOMS), 27*(3), 299-316. [CrossRef]

[32] Subhas Abel, M., Tawade, J. V., & Nandeppanavar, M. M. (2012). MHD flow and heat transfer for the upper-convected Maxwell fluid over a stretching sheet. *Meccanica, 47*(2), 385-393. [CrossRef]

[33] Megahed, A. M. (2013). Variable fluid properties and variable heat flux effects on the flow and heat transfer in a non-Newtonian Maxwell fluid over an unsteady stretching sheet with slip velocity. *Chinese Physics B, 22*(9), 094701. [CrossRef]

[34] Waqas, M., Khan, M. I., Hayat, T., & Alsaedi, A. (2017). Stratified flow of an Oldroyd-B nanoliquid with heat generation. *Results in Physics, 7*, 2489-2496. [CrossRef]

[35] Irfan, M., Khan, M., & Khan, W. A. (2019). Impact of homogeneous–heterogeneous reactions and non-Fourier heat flux theory in Oldroyd-B fluid with variable conductivity. *Journal of the Brazilian Society of Mechanical Sciences and Engineering, 41*(3), 135. [CrossRef]

[36] Ahmed, A., Alhowaity, S., Ghoneim, M. E., Gamaoun, F., Tag-eldin, E., Yassen, M. F., & Sarfraz, M. (2022). Material and wave relaxation phenomena effects on the rheology of Maxwell nanofluids. *Frontiers in Physics, 10*, 1005056. [CrossRef]

K. Sudarmozhi is an Assistant Professor (Senior Grade) in the Department of Mathematics, Saveetha School of Engineering, Saveetha Institute of Medical and Technical Sciences (SIMATS), Chennai, India. She received the Ph.D. degree in Mathematics and also holds B.Sc., M.Sc., M.Phil. and PGDCA qualifications. Her research interests include fluid dynamics, heat and mass transfer, and Maxwell fluid flow. She has more than thirteen years of teaching and research experience, supervises four doctoral scholars and serves as a reviewer for several international journals. (Email: sudarmozhik1033.sse@saveetha.com)